

Impact of chirality imbalance and nonlocal interactions on the QCD-biased axionic domain-wall interpretation of NANOGrav 15-year data

Ruotong Zhao¹ and Zhao Zhang^{1,*}

¹*School of Mathematics and Physics, North China Electric Power University, Beijing 102206, China*
(Dated:)

We investigate the influence of the chirality imbalance with local CP-breaking in hot QCD on the generation of a stochastic gravitational wave background (SGWB) sourced by the axion-like particle (ALP) domain-wall annihilation, induced by the QCD bias. Such a bias is quantified by the QCD topological susceptibility χ_t , and its dependence on the θ angle and the chiral chemical potential μ_5 is investigated at temperatures near the QCD scale within a nonlocal Nambu–Jona-Lasinio (NJL) model. We find that, besides the small- θ range, the axionic domain-wall interpretation of NANOGrav 15-year data on the nHz gravitational waves is still possible for a certain large- θ range if μ_5 is large enough. We confirm that the peak of $|\chi_t|$ at the critical temperature T_c for the CP restoration at $\theta = \pi$ exhibits a pronounced width compared to the local NJL result. Thus, for θ at and around π , the QCD bias near T_c can also produce a GW signal strength compatible with the NANOGrav 15-year data.

PACS numbers: 12.38.Aw, 12.38.Mh

Keywords: Nanohertz gravitational waves, Domain wall, Topological susceptibility, Chiral chemical potential, QCD phase transition

I. INTRODUCTION

Gravitational wave (GW) research has opened a new era in the exploration of the mysteries of the Universe. In recent years, significant breakthroughs have been achieved in the study of low-frequency (nHz) GW through the pulsar timing arrays (PTA). The NANOGrav collaboration, after 15 years of data collection, has reported observations of the SGWB [1–3]. Other recent PTA datasets—including those from the European PTA (EPTA) [4–6], the Parkes PTA (PPTA) [7, 8], and the Chinese PTA (CPTA) [9]—also provide consistent evidence supporting the existence of nHz stochastic GWs.

Identifying sources of the SGWB in the nHz band opens up new avenues for revealing the early Universe and exploring the new physics beyond the Standard Model (BSM) [2, 10]. Besides the strong candidate of supermassive black hole binaries [3, 11, 12], the proposed new physics sources include cosmic first-order phase transitions [13–17], cosmic strings [18–22], domain walls (DMs) [23–26], inflation [27–31], scalar-induced GWs [32–36], and other astrophysical and cosmological ones [37–41]. In this work, we focus on the possibility that the nHz range GW is sourced by the DM collapse stemmed from the ALP due to the QCD bias.

Domain walls are the two-dimensional topological defects and a wall serves as a boundary separating regions of space with different degenerate vacuum states. In the early Universe, DWs may form due to the spontaneous breaking of the discrete symmetry [42]. The stable DMs pose a cos-

mological problem [43]: their energy density decreases more slowly than that of radiation and matter and would eventually overwhelm all other energy components as the Universe expands, leading to a cosmological scenario that is completely incompatible with our observed Universe [44]. A mechanism to prevent DMs from dominating the Universe’s energy is to introduce a bias potential to break the vacuum degeneracy and promote the annihilation of the DM network. Since DMs are two-dimensional, their collapse is typically associated with violent and asymmetric spacetime disturbances, leading to the generation of GWs.

DWs inherently emerge in models with ALPs, which are generalizations of the Peccei–Quinn axion addressing the strong CP problem [45–47] and are widely motivated in the theories BSM [48–50]. As light scalars, axion and ALP are also the compelling candidates for dark matter. As a cosmological source of GWs, the ALP-DM annihilation induced by a QCD bias has been considered as an attractive scenario [51–58], which can naturally realize a peak frequency in the nHz band during the QCD phase transition at $T \sim \mathcal{O}(100)\text{MeV}$ [2]. In this formalism, the QCD-induced bias is provided by the topological susceptibility χ_t , a fundamental quantity measuring how the QCD vacuum responds to the topological charge fluctuations. The T -dependence of χ_t has been investigated in lattice QCD simulations [59] and the corresponding results have been used in the previous calculations [53–55]. Note that the possible CP-odd effect in hot QCD matter is ignored in these studies.

At very high temperature, the sphaleron transition [60, 61] in the electroweak theory has been investigated as a mechanism for baryogenesis [62–66]. Similarly, local CP-odd domains may arise in the hot QCD plasma via strong sphaleron transitions [67]. Previous studies suggest that, for

* zhaozhang@pku.org.cn

high temperature, the gluon configurations with nonzero winding number can be created with relatively high probability [67–72]. This implies the QCD vacuum characterized by nonzero θ angle and its fluctuation may become sufficiently sizable and even lead to direct experimental signatures [73, 74]. Recently, the impact of a local CP-odd domain in hot QCD on the axion DM interpretation of NANOGrav 15-year data (NG15) has been performed by considering a finite θ within the NJL formalism [75]. The main conclusion obtained is that the GW signal strength from the axionic DM collapse due to a QCD bias may not be consistent with the NG15 due to the significant suppression of χ_t by the θ parameter of order one. In particular, it is found in [75] that the magnitude of χ_t tends to become significantly large at $\theta = \pi$ due to criticality, but the bias leads to too large signal strength to be compatible with the NG15 data.

Note that in the local CP-odd domain of hot QCD, the chirality imbalance emerges naturally due to the axial anomaly. Typically, the chiral chemical potential μ_5 , which corresponds to the time derivative of θ ¹, is introduced to quantify the chirality imbalance [74]. It is well known that such an imbalance may lead to chiral magnetic effect in heavy-ion collisions [73, 74]. Owing to QCD sphalerons, the chirality imbalance may become substantial within the QCD timescale at the early Universe. According to the lattice QCD calculation [76–78], the chiral condensate (thus also χ_t) is enhanced significantly by a large μ_5 . This means the chirality imbalance tends to promote the QCD bias toward the axion DM collapse. Such a catalytic effect on χ_t due to the chirality imbalance is not taken into account in Ref. [75], where the CP-odd effect is solely described by a nonzero θ .

In this work, we focus on whether the GW signal strengths generated from the axionic DM collapse induced by QCD bias in a local CP-odd domain are consistent with the NG15 data by simultaneously considering the nonzero μ_5 and θ . Different from [75], a nonlocal two-flavor NJL (NNJL) model with 't Hooft interaction [79–87] is adopted in our calculation. The first reason for such a model choice is that the local NJL used in [75] fails to yield the results qualitatively consistent with the lattice QCD calculation at finite μ_5 , whereas the NNJL can do [83, 84]. Another is that the NNJL model better captures non-perturbative features of QCD, such as the nonlocal quark–gluon coupling and confinement-related dynamics, which may give more reasonable results at finite θ , especially at the critical point $\theta = \pi$ for the thermal CP restoration.

As in Refs. [22, 75], we assume that the axionic DMs are induced by the spontaneous breaking of Z_2 symmetry, where a small Z_2 breaking potential

is a necessary condition for making the DM unstable. We propose that this Z_2 breaking potential is induced by the coupling between the ALP and gluons [22, 75] via the axial anomaly during the QCD epoch. Through this approach, we can calculate the DM tension and the bias potential; these results allow us to evaluate the signal strengths of generated GWs and compare them with the NG15 dataset.

The rest of this paper is organized as follows. In section II, we present the general scenario of the axion DMs and its collapse due to the QCD-induced bias. In section III, we describe the NNJL model at finite θ and μ_5 and show the method to calculate the QCD bias and the axion domain wall energy density within this formalism. In section IV, we compare the numerical results with the NANOGrav’s 15-year observational data and provide relevant discussions. The conclusion and outlook are presented in section V.

II. AXIONIC DOMAIN WALLS WITH QCD BIAS

A. Axionic domain walls and QCD-bias potential

Following [26, 52–58], the ALP a is assumed to present prior to the QCD phase transition and a potential

$$V_0(a) = \frac{m_a^2 f_a^2}{n^2} \left(1 - \cos \left(n \frac{a}{f_a} \right) \right) \quad (1)$$

had already been developed by some non-perturbative effects [26, 52, 75, 88]. Here, m_a and f_a refer to the mass and decay constant of the ALP, respectively, while the integer n denotes the DW number. Clearly, the potential (1) satisfies the periodic condition

$$a/f_a \rightarrow a/f_a + 2\pi \quad (2)$$

and has degenerate minima at $a/f_a = 2\pi k/n$ where k is an integer. This means there are n degenerate distinct vacuum states and there exist the DM configurations interpolating between the adjacent vacua $a/f_a = 2\pi k/n$ and $2\pi(k+1)/n$. The tension of such a DW [88] is

$$\sigma = \frac{8}{n^2} m_a f_a^2. \quad (3)$$

In the context of the axion models, the potential (1) breaks the $U(1)_{PQ}$ symmetry down to the discrete Z_n subgroup, leading to the formation of stable DWs for $n \geq 2$.

As the Universe approaches the QCD scale, an additional potential induced by the $U(1)_A$

¹ In general, the parameter θ is time and space dependent.

anomaly of QCD emerges with the form [22, 75]

$$V_{\text{QCD}}(a) = \chi_t(T, \theta, \mu_5) \left(1 - \cos \left(n_g \frac{a}{f_a} + \theta \right) \right), \quad (4)$$

where n_g is a factor related to Peccei-Quinn charges of quarks. Note that in our case, the topological susceptibility is dependent on T , μ_5 , and θ .

Typically, it is assumed $m_a^2 f_a^2 \gtrsim |\chi_t|$. The total potential takes the form

$$\begin{aligned} V_{\text{total}}(a) &= V_0(a) + V_{\text{QCD}}(a) \\ &= \frac{m_a^2 f_a^2}{n^2} \left(1 - \cos \left(n \frac{a}{f_a} \right) \right) \\ &\quad + \chi_t \left(\cos \theta - \cos \left(n_g \frac{a}{f_a} + \theta \right) \right). \end{aligned} \quad (5)$$

which is normalized with the condition $V_{\text{total}}(a = 0) = 0$. In this context, $V_{\text{QCD}}(a)$ serves as the bias term, which breaks the Z_n symmetry explicitly. For $n \geq 2$, DMs become unstable and collapse when the bias is large enough, releasing latent heat into the Universe.

Following [22, 75], we choose $n = 2$ and $n_g = 1$. In this case, the vacuum degeneracy lifting happens due to the bias potential. The original vacuum at $a/f_a = \pi$ gets the energy shift by

$$\begin{aligned} \Delta V &= \left| V_{\text{total}} \Big|_{\frac{a}{f_a}=\pi} - V_{\text{total}} \Big|_{\frac{a}{f_a}=0} \right| \\ &= |V_0 + V_{\text{QCD}} \Big|_{\frac{a}{f_a}=\pi} \\ &= |\chi_t(T, \mu_5, \theta) (\cos(\pi + \theta) - \cos \theta)| \\ &= |C(\theta) \chi_t(T, \mu_5, \theta)| \end{aligned} \quad (6)$$

compared to that at $a/f_a = 0$, where $C(\theta) = 2 \cos \theta^2$.

The DMs begin to collapse when the potential bias ΔV is comparable to the DM energy density $\rho_{\text{DW}}(T, \mu_5, \theta)$. This means that the maximal amount of the released latent heat corresponds to $\rho_{\text{DW}}(T)$

$$\rho_{\text{DW}} \sim \Delta V(T, \mu_5, \theta) = |C(\theta) \chi_t(T, \mu_5, \theta)|. \quad (7)$$

In the following, we will adopt the numerical analysis result

$$\rho_{\text{DW}} \simeq 0.5 \Delta V \quad (8)$$

obtained in [88, 89].

B. GWs from DW network collapse

We assume that the axionic DM annihilation due to the QCD bias happens at $T = T_*$ and is the only source of the GW. The produced GW power spectrum at the peak frequency is then assessed via the following signal strength [52]

$$\begin{aligned} \alpha_*(T_*, \mu_5, \theta) &= \frac{\rho_{\text{DW}}(T_*)}{\rho_{\text{rad}}(T_*)} \simeq \frac{0.5 \Delta V(T_*, \theta)}{\rho_{\text{rad}}(T_*)} \\ &\simeq 0.15 \times \left(\frac{|C(\theta) \chi_t(T_*, \mu_5, \theta)|^{1/4}}{100 \text{ MeV}} \right)^4 \\ &\quad \times \left(\frac{T_*}{100 \text{ MeV}} \right)^{-4} \left(\frac{g_*(T_*)}{10} \right)^{-1}, \end{aligned} \quad (9)$$

where $g_*(T_*)$ is the effective number of relativistic degrees of freedom at $T = T_*$ and

$$\rho_{\text{rad}}(T) = \frac{\pi^2}{30} g_*(T) T^4. \quad (10)$$

We will compute the signal strength α_* by evaluating the topological susceptibility within the NNJL model and compare it with the NG15 dataset. As in Ref. [75], the effective degrees of freedom $g_*(T)$ near the QCD phase transition temperature are taken from Ref. [90].

III. NNJL MODEL ANALYSIS OF χ_t AND AXIONIC DW ENERGY DENSITY AT NONZERO θ AND μ_5

A. The formalism

The non-perturbative formalism we used to calculate the QCD bias is the type of two flavor NNJL model, which has been extensively used to investigate the QCD phase transition at finite temperature and baryon density [79–87]. In the QCD Lagrangian, the topological angle θ appears as a CP-odd term

$$\delta \mathcal{L}_\theta = \theta q(x) = \theta \frac{g^2}{32\pi^2} G_{\mu\nu}^a(x) \tilde{G}^{\mu\nu,a}(x), \quad (11)$$

where $G_{\mu\nu}^a(x)$ is the gluon field strength tensor and $\tilde{G}^{\mu\nu,a}(x) = \frac{1}{2} \epsilon_{\mu\nu\rho\sigma} G^{\rho\sigma,a}(x)$ is its dual, and $q(x)$ is the topological charge density. In the NJL formalism, the angle θ can be introduced via the instanton induced quark interactions.

We adopt the two flavor NNJL model used in Ref. [84], which Lagrangian density includes three terms

$$\mathcal{L} = \mathcal{L}_q + \mathcal{L}_m + \mathcal{L}_4. \quad (12)$$

The first is

$$\mathcal{L}_q = \bar{\psi} (i \gamma^\mu \partial_\mu + \mu_5 \gamma^0 \gamma^5) \psi, \quad (13)$$

² Note that the coefficient $C(\theta)$ is ignored in the corresponding formula of the potential bias in Ref. [75].

which denotes the free quark contribution with the chiral chemical potential μ_5 . The second is the mass term

$$\mathcal{L}_m = -m_0 \bar{\Psi} \Psi, \quad (14)$$

where m_0 is the current quark mass. Note that the dressed quark field

$$\Psi(x) = \int d^4y G(x-y)\psi(y) \quad (15)$$

is introduced in (14), where $G(x-y)$ denotes an formfactor. Using this special form of (14) rather than the standard one $\mathcal{L}_m^{(0)} = -m_0 \bar{\psi} \psi$ aims to mimic the perturbative tail of the current quark mass at large Euclidean momentum [84]. The last is the term of nonlocal four-quark interactions

$$\begin{aligned} \mathcal{L}_4 = G_1 \sum_{\ell=0}^3 [(\bar{Q}\tau_\ell Q)^2 + (\bar{Q}i\gamma^5\tau_\ell Q)^2] \\ + 8G_2 [e^{i\theta} \det(\bar{Q}_R Q_L) + e^{-i\theta} \det(\bar{Q}_L Q_R)], \end{aligned} \quad (16)$$

where $\tau_l = (\mathbb{1}, i\boldsymbol{\tau})$ is a quaternion in flavor space and the spinor Q denotes another dressed quark field

$$Q(x) = \int d^4y F(x-y)\psi(y), \quad (17)$$

defined via the form factor $F(x-y)$. The first part of the interactions (16) represents the nonlocal coupling between scalar (pseudoscalar) bilinears of the quark fields, which respects chiral symmetry; The second is the nonlocal 't Hooft interaction induced by QCD instantons, which violates the $U(1)_A$ symmetry. As mentioned, the nonzero angle θ appears in this term, indicating the breaking of strong CP symmetry.

The form factors $G(x-y)$ and $F(x-y)$ in (15) and (17) will be specified later. Clearly, the local NJL corresponds to the case with $F(x-y) = \delta(x-y)$, which has been adopted to study properties of QCD axion in Ref. [91]. In all forms, we have $G_1 = (1-c)G$, $G_2 = cG$ and $c = 0.2$ [91].

The explicit θ dependence in (16) can be removed by performing the chiral rotation

$$\psi_R \rightarrow e^{-i\theta/4}\psi_R \equiv \psi'_R, \quad \psi_L \rightarrow e^{i\theta/4}\psi_L \equiv \psi'_L, \quad (18)$$

and the Lagrangian (16) turns into

$$\begin{aligned} \mathcal{L}'_4 = G_1 \sum_{\ell=0}^3 [(\bar{Q}'\tau_\ell Q')^2 + (\bar{Q}'i\gamma^5\tau_\ell Q')^2] \\ + 8G_2 [\det(\bar{Q}'_R Q'_L) + \det(\bar{Q}'_L Q'_R)] \end{aligned} \quad (19)$$

with

$$Q'(x) = \int d^4y F(x-y)\psi'(y). \quad (20)$$

Consequently, the θ parameter appears in the quadratic part of the Lagrangian (12) and the mass term becomes

$$\mathcal{L}'_m = -\bar{\Psi}'(m_{0+} + im_{0-}\gamma^5)\Psi', \quad (21)$$

where

$$\Psi'(x) = \int d^4y G(x-y)\psi'(y), \quad (22)$$

$$m_{0+} = m_0 \cos(\theta/2), \quad m_{0-} = m_0 \sin(\theta/2). \quad (23)$$

Following Ref. [84], we also introduce the collective fields in the primed bilinear forms

$$\sigma' = G_+ \bar{Q}' Q', \quad (24)$$

$$\eta' = G_- \bar{Q}' i\gamma^5 Q', \quad (25)$$

where $G_\pm = G_1 \pm G_2$. The corresponding original bilinear fields can be obtained via the orthogonal rotation

$$\begin{pmatrix} \bar{Q} Q \\ \bar{Q} i\gamma^5 Q \end{pmatrix} = \begin{pmatrix} \cos \frac{\theta}{2} & \sin \frac{\theta}{2} \\ -\sin \frac{\theta}{2} & \cos \frac{\theta}{2} \end{pmatrix} \begin{pmatrix} \bar{Q}' Q' \\ \bar{Q}' i\gamma^5 Q' \end{pmatrix}. \quad (26)$$

We use σ'_0 (η'_0) to denote the vacuum condensate of the field σ' (η'). The mean field thermodynamic potential at the one-loop approximation for finite T , μ_5 , and θ takes the form

$$\begin{aligned} \Omega_M = \frac{\sigma'^2_0}{G_+} + \frac{\eta'^2_0}{G_-} \\ - 2N_c T \sum_n \int \frac{d^3p}{(2\pi)^3} \log [\beta^4 (\omega_n^2 + E_+^2) \\ \times (\omega_n^2 + E_-^2)], \end{aligned} \quad (27)$$

where $\beta = 1/T$ and $\omega_n = (2n+1)\pi T$ are the Matsubara frequencies for quark fields. The energy branches E_\pm in Eq. (27) are defined as

$$E_\pm^2(p) = (|\mathbf{p}| \pm \mu_5)^2 + \mathcal{M}^2(p) + \mathcal{N}^2(p), \quad (28)$$

where $p \equiv |\mathbf{p}|$ and the two momentum dependent masses read

$$\mathcal{M}(p) = m_{0+} \mathcal{R}(p) - 2\mathcal{C}(p)\sigma'_0, \quad (29)$$

$$\mathcal{N}(p) = m_{0-} \mathcal{R}(p) - 2\mathcal{C}(p)\eta'_0. \quad (30)$$

The functions $\mathcal{C}(p)$ and $\mathcal{R}(p)$ are defined as

$$\mathcal{C}(p) \equiv F^2(p), \quad (31)$$

$$\mathcal{R}(p) \equiv G^2(p), \quad (32)$$

where $F(p)$ ($G(p)$) is the Fourier transform of the form factor $F(x-y)$ ($G(x-y)$).

The condensates σ'_0 and η'_0 are determined by the stationary condition

$$\frac{\partial \Omega_M}{\partial \sigma'_0} = \frac{\partial \Omega_M}{\partial \eta'_0} = 0. \quad (33)$$

The related original two condensates can be obtained by the transition

$$\begin{pmatrix} \langle \bar{Q} Q \rangle \\ \langle \bar{Q} i\gamma^5 Q \rangle \end{pmatrix} = \begin{pmatrix} \cos \frac{\theta}{2} & \sin \frac{\theta}{2} \\ -\sin \frac{\theta}{2} & \cos \frac{\theta}{2} \end{pmatrix} \begin{pmatrix} \sigma'_0/G_+ \\ \eta'_0/G_- \end{pmatrix}. \quad (34)$$

B. The model parameters

In this paper, we utilize three different sets of analytical forms of $\mathcal{R}(p)$ and $\mathcal{C}(p)$ which had been extensively used in the previous studies.

The first set is taken from Refs. [83, 84] with

$$\begin{aligned} \mathcal{C}(p_E) &= \theta(\Lambda^2 - p_E^2) \\ &+ \theta(p_E^2 - \Lambda^2) \frac{\Lambda^2 (\log \Lambda^2 / \Lambda_{\text{QCD}}^2)^\gamma}{p_E^2 (\log p_E^2 / \Lambda_{\text{QCD}}^2)^\gamma} \end{aligned} \quad (35)$$

and

$$\begin{aligned} \mathcal{R}(p_E) &= \theta(\Lambda^2 - p_E^2) \\ &+ \theta(p_E^2 - \Lambda^2) \frac{(\log \Lambda^2 / \Lambda_{\text{QCD}}^2)^{d_m}}{(\log p_E^2 / \Lambda_{\text{QCD}}^2)^{d_m}}. \end{aligned} \quad (36)$$

Here p_E refers to the Euclidean 4-momentum and $\gamma = 1 - d_m$. The parameter $d_m = 12/29$ is the anomalous dimension of the current quark mass for a two-flavor QCD.

The second is adopted from Refs. [83, 85, 92] with

$$\mathcal{C}(p_E) = \exp(-p_E^2 / \Lambda^2) \quad (37)$$

and

$$\mathcal{R}(p_E) = 1. \quad (38)$$

Clearly, the form factor $G(x - y)$ is simplified to $\delta^{(4)}(x - y)$ in this model.

The third is taken from Refs. [86, 87] with

$$\mathcal{C}(p_E) = -\frac{g^2}{G} \frac{B_0}{p_E^2 + M_0^2} \quad (39)$$

and also

$$\mathcal{R}(p_E) = 1. \quad (40)$$

Here, B_0 and M_0 are the first terms of the two sequences

$$B_n = (2n + 1) \frac{\pi^2}{K^2(i)} \frac{(-1)^{n+1} e^{-(n+\frac{1}{2})\pi}}{1 + e^{-(2n+1)\pi}}, \quad (41)$$

and

$$M_n = \left(n + \frac{1}{2}\right) \frac{\pi}{K(i)} \left(\frac{Ng^2}{2}\right)^{\frac{1}{4}} \Lambda, \quad (42)$$

with n being an integer, $K(i) \approx 1.3111028777$, $g = 3$, and $N = 3$, respectively.

The effective momentum cutoff parameter Λ in all three sets of $\mathcal{C}(p)$ is fixed by reproducing the vacuum quark condensate and pion decay constant

in combination with the coupling G and current quark mass m_0 . For convenience, the three versions of NNJL are referred to as NNJL I-III, respectively. The corresponding three sets of the parameter m_0 , G , and Λ are listed in Table I, which are taken from Refs. [84], [92], and [86], respectively.

C. Evaluation of topological susceptibility in NNJL

The QCD topological susceptibility χ_t at finite θ is defined as

$$\begin{aligned} \chi_t &= \frac{1}{V} \langle Q^2 \rangle = \int d^3x \langle q(0)q(x) \rangle_\theta \\ &= \left. \frac{d^2 \Omega_{\text{QCD}}}{d\theta^2} \right|_\theta. \end{aligned} \quad (43)$$

In the NNJL formalism, the topological susceptibility can be evaluated via

$$\chi_t = \left. \frac{d^2 V}{d\theta^2} \right|_\theta, \quad (44)$$

where V is an effective potential³ defined as

$$V(T, \theta, \mu_5) = \Omega_m(x_i(T, \theta, \mu_5), T, \theta, \mu_5), \quad (45)$$

and $x_i(T, \theta, \mu_5)$ refer to the physical values of σ'_0 and η'_0 , which are solutions of the gap equations (33) at given T , θ , and μ_5 . Since the physical condensates are all implicitly dependent on θ , the total differential of $V(\theta)$ with respect to θ satisfies the following relation

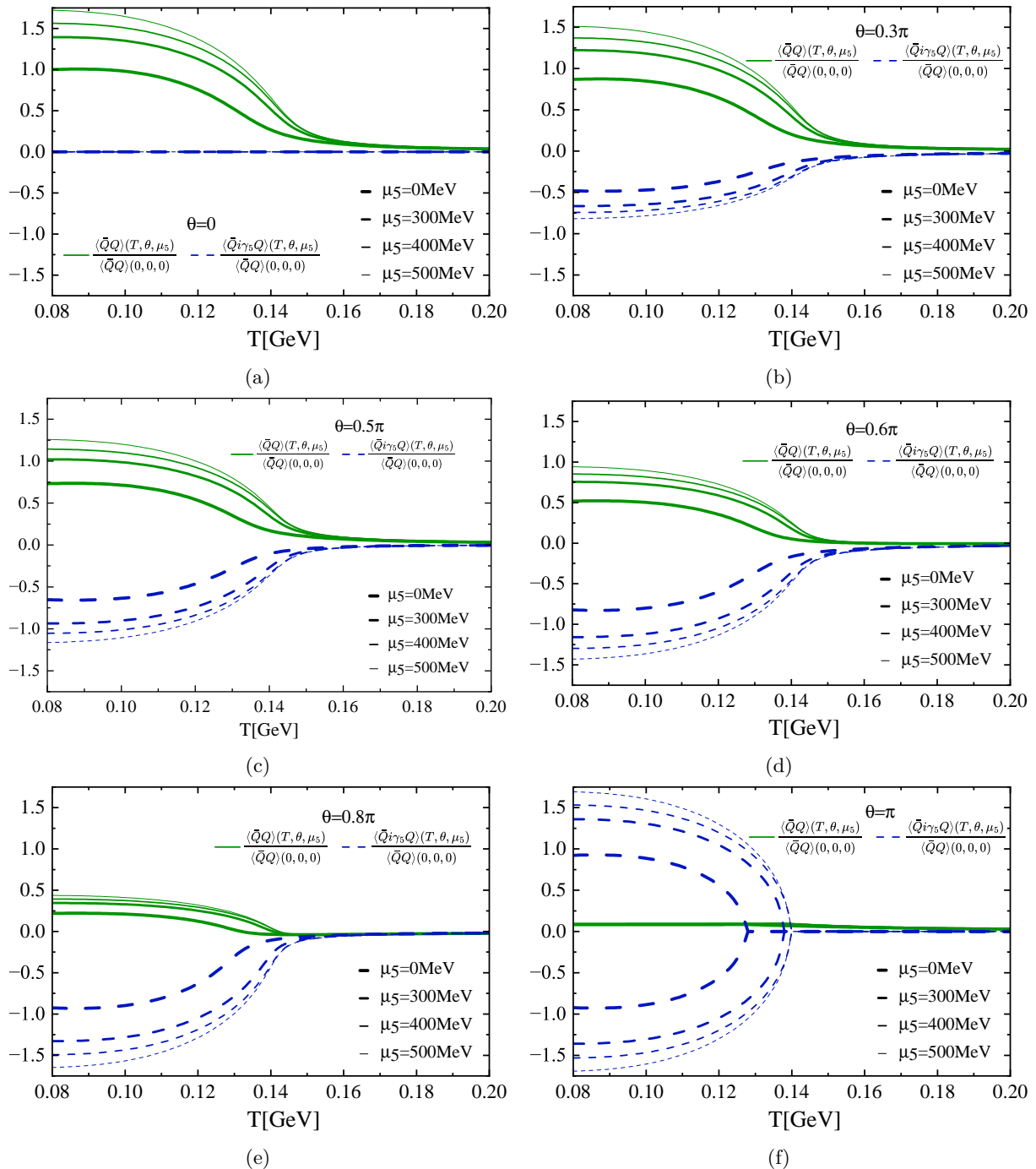
$$\frac{dV}{d\theta} = \frac{\partial V}{\partial \theta} + \frac{\partial V}{\partial \sigma'_0} \frac{\partial \sigma'_0}{\partial \theta} + \frac{\partial V}{\partial \eta'_0} \frac{\partial \eta'_0}{\partial \theta}. \quad (46)$$

Therefore to calculate χ_t , we need to compute the 1-2th partial derivatives of each of the physical condensates with respect to θ , namely $\left. \frac{\partial^{(n)} x_i}{\partial \theta^{(n)}} \right|_\theta$, where $n = 1, 2$. This can be fulfilled by taking the successive derivatives of the gap equations (33) with respect to θ . First, the system of linear equations with $\frac{\partial x_i}{\partial \theta}$ as variables can be obtained by differentiating the gap equations (33) with respect of θ and thus $\left. \frac{\partial x_i}{\partial \theta} \right|_\theta$ can be calculated using the numerical solutions of (33) at θ . Second, the linear equations with $\frac{\partial^{(2)} x_i}{\partial \theta^{(2)}}$ as variables can be obtained by taking the second-order derivative of (33) with respect to θ and then $\left. \frac{\partial^{(2)} x_i}{\partial \theta^{(2)}} \right|_\theta$ can be computed (since $x_i|_\theta$ and $\left. \frac{\partial x_i}{\partial \theta} \right|_\theta$ are all known). Such a method has been used to evaluate the mass and self-coupling of QCD axion within the NJL framework [93, 94].

³ It corresponds to the potential of QCD axion if θ is replaced by the axion field a/f_a .

TABLE I: Model parameters

model	m_0 [MeV]	Λ [MeV]	G	$\langle\bar{\psi}\psi\rangle$ [(MeV) ³]	Λ_{UV} [MeV]
NNJL I	5	550	$2.6/\Lambda^2$	$(-250)^3$	3Λ
NNJL II	5.8	902.4	$15.82/\Lambda^2/2$	$(-240)^3$	10Λ
NNJL III	3.3	770	$7.0686/440^2/2(\text{MeV})^{-2}$	$(-250)^3$	3Λ

FIG. 1: Normalized scalar and pseudoscalar condensates versus temperature for different μ_5 and θ . The data are obtained using NNJL I.

IV. NUMERICAL RESULTS AND DISCUSSION

We show the numerical results in this section. We mainly concentrate on the situation with a rel-

atively larger μ_5 (we assume $\mu_5 > 0$), which may exert a significant impact on the QCD bias.

The normalized condensates $\langle\bar{Q}Q\rangle$ and $\langle\bar{Q}i\gamma_5 Q\rangle$

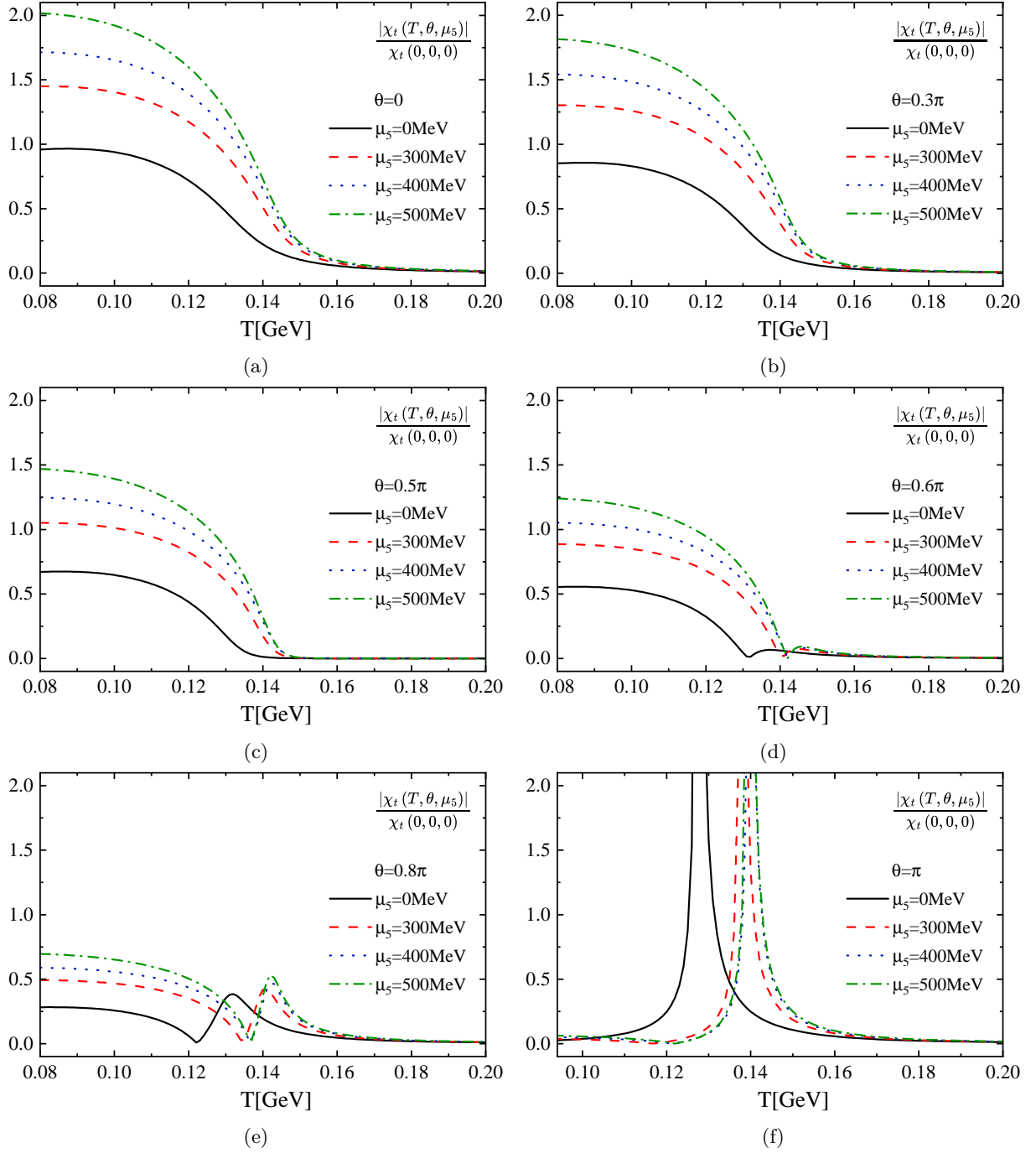


FIG. 2: Absolute value of topological susceptibility χ_t versus temperature under the same conditions as that in Fig. 1.

as functions of T are shown in Fig. 1 for $\theta \in [0, \pi]$ with fixed $\mu_5 = 300, 400, 500$ MeV, with all results calculated in NNJL I. Panel (a) displays that for zero θ , the scalar condensate $|\langle \bar{Q}Q \rangle|$ increases with μ_5 ⁴, which is consistent with Refs. [83, 84]. Panels (b)-(f) demonstrate that for nonzero θ , not

⁴ Consistent with the lattice results, there is no so called inverse catalytic effect near the crossover temperature obtained in the local NJL.

only $|\langle \bar{Q}Q \rangle|$, but also the pseudo-scalar condensate $|\langle \bar{Q}i\gamma_5 Q \rangle|$ get larger with μ_5 . Panel (f) illustrates Danshen's phenomenon at $\theta = \pi$: the condensate $\langle \bar{Q}i\gamma_5 Q \rangle$ exhibits two degenerate solutions with opposite signs at low temperature, signaling the spontaneous CP symmetry breaking. We see that the CP restoration temperature also increases with μ_5 due to the catalytic effect of chirality imbalance.

The magnitude of the normalized χ_t versus T under the same conditions as in Fig. 1 is demon-

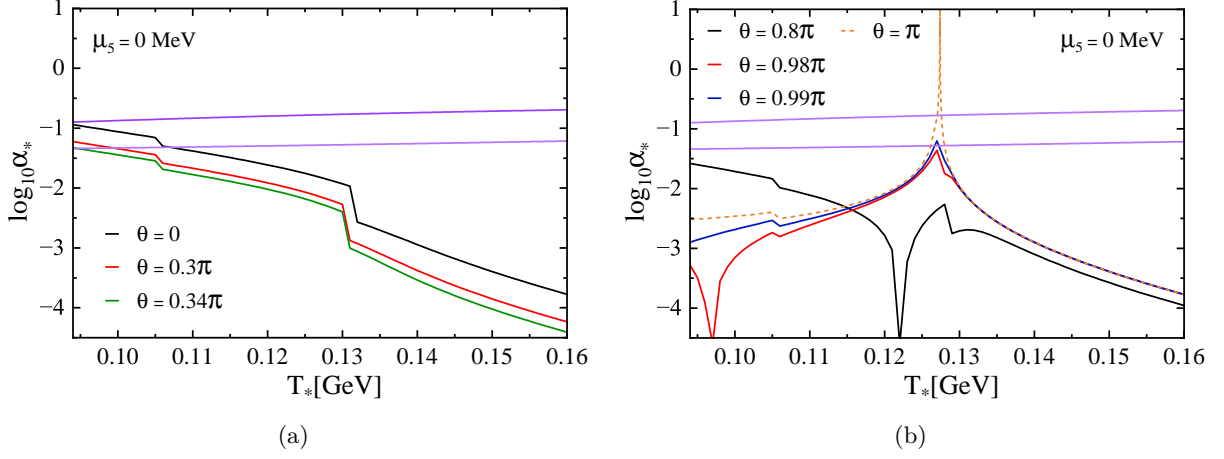


FIG. 3: The signal strength $\alpha_*(T_*, \theta, \mu_5)$ versus the axionic DM annihilation temperature T_* for different θ at $\mu_5 = 0$ MeV, calculated within NNJL I. The lines for $0 \leq \theta < 0.5\pi$ ($0.5\pi < \theta \leq \pi$) are shown in the left (right) panel. The two purple lines correspond to the 2σ contour from Ref.[2], with the region inside denoting the allowed parameter space for the nHz GWs. Left panel: $0 \leq \theta \leq 0.34\pi$; right panel: $0.98\pi \leq \theta \leq \pi$ can access the two-line regime.

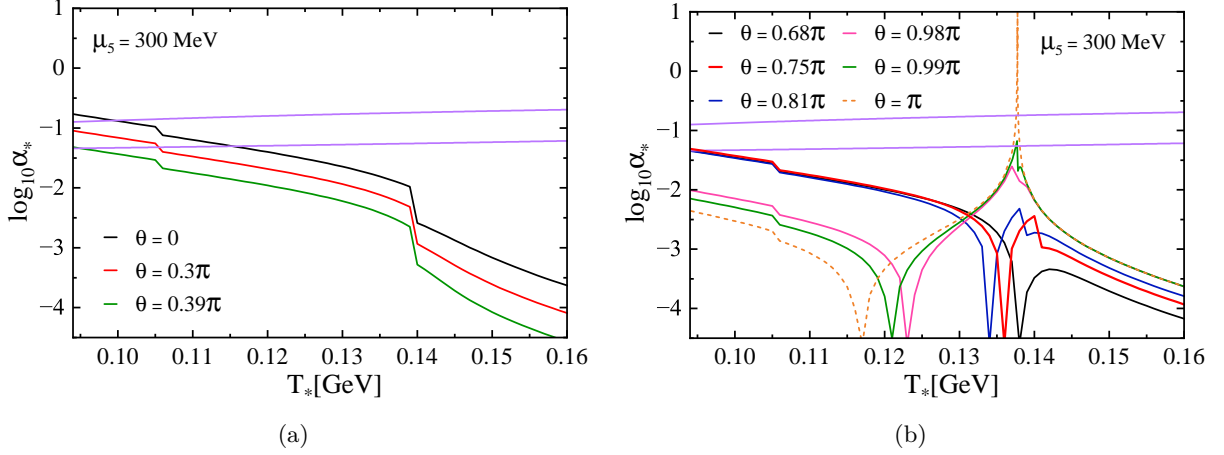


FIG. 4: Same as in Fig. 3, but for $\mu_5 = 300$ MeV. Left panel: $0 \leq \theta \leq 0.39\pi$; right panel: $0.68\pi \leq \theta \leq 0.81\pi$ and $0.98\pi \leq \theta \leq \pi$ can access the two-line regime.

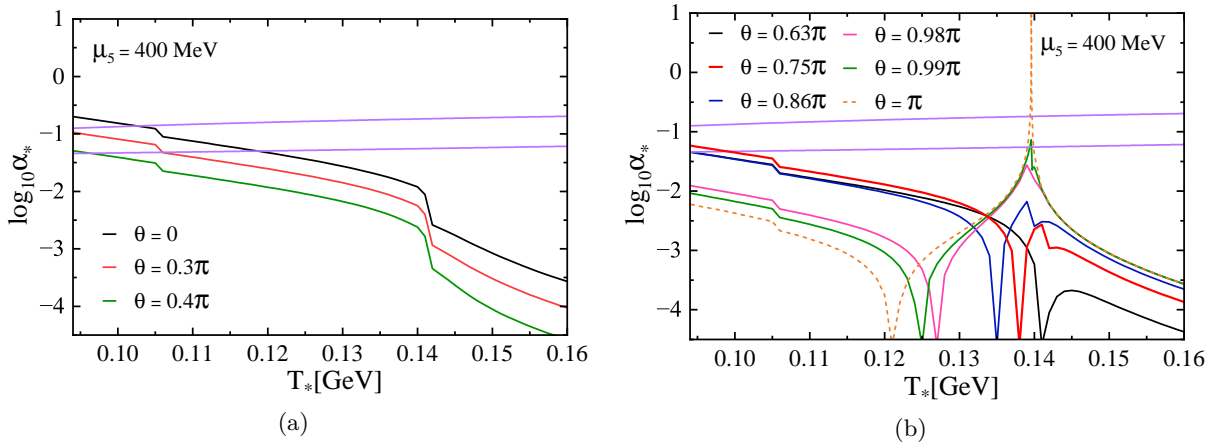


FIG. 5: Same as in Fig. 3, but for $\mu_5 = 400$ MeV. Left panel: $0 \leq \theta \leq 0.4\pi$; right panel: $0.63\pi \leq \theta \leq 0.86\pi$ and $0.98\pi \leq \theta \leq \pi$ can access the two-line regime.

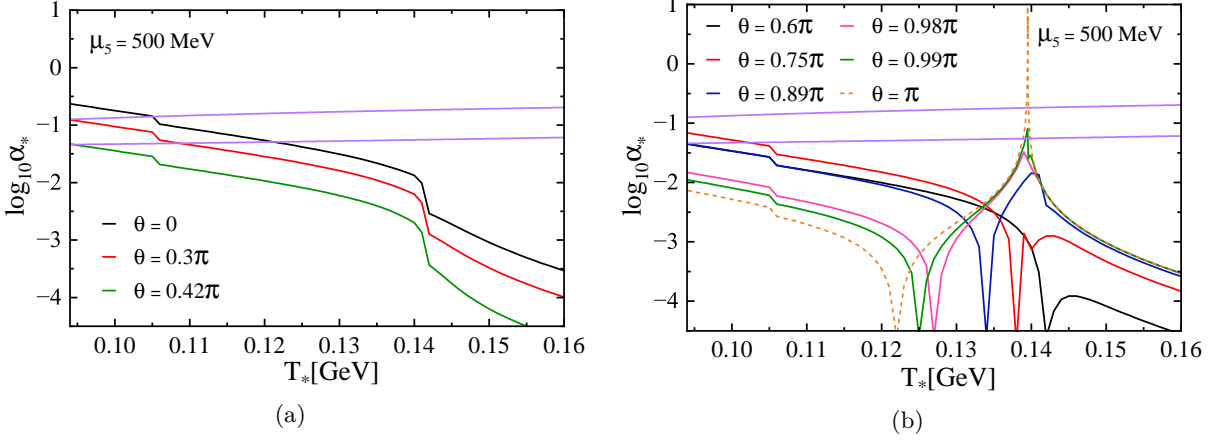


FIG. 6: Same as in Fig. 3, but for $\mu_5 = 500$ MeV. Left panel: $0 \leq \theta \leq 0.42\pi$; right panel: $0.6\pi \leq \theta \leq 0.89\pi$ and $0.98\pi \leq \theta \leq \pi$ can access the two-line regime.

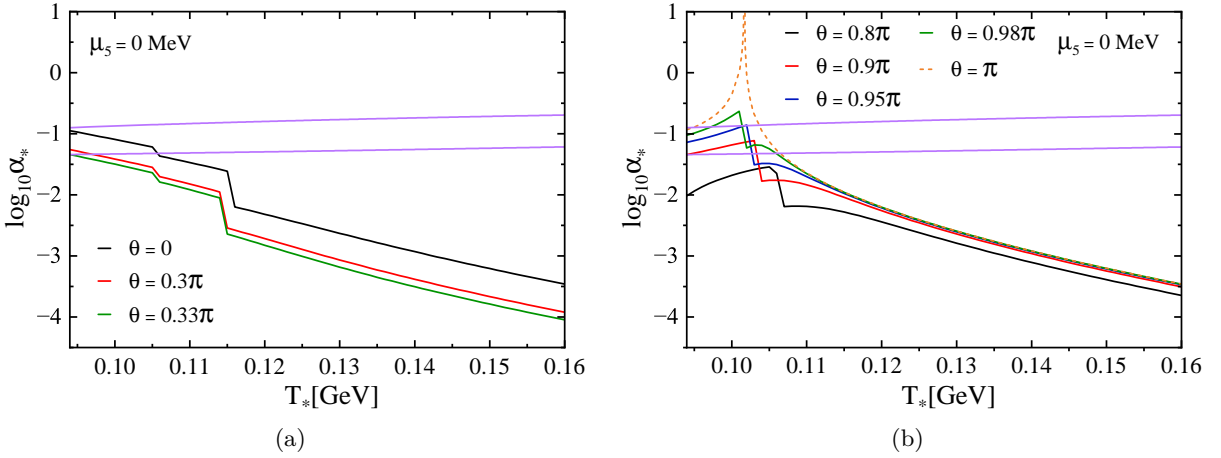


FIG. 7: Same as in Fig. 3, but within NJJL II. Left panel: $0 \leq \theta \leq 0.33\pi$; right panel: $0.9\pi \leq \theta \leq \pi$ can access the two-line regime.

strated in Fig. 2. Panels (a)-(c) show that χ_t always decreases with T for fixed μ_5 and $\theta \leq 0.5\pi$, and is enhanced (suppressed) by μ_5 (θ) for fixed T and θ (μ_5). We see that at low temperatures, the χ_t at $\mu_5 = 500$ MeV is roughly twice that at zero μ_5 for all three θ angles. Panels (d)-(e) display that for a relatively larger $\theta = 0.6\pi, 0.8\pi$, the absolute value of χ_t first falls to zero with increasing T , then increases to a local maximum and gradually declines thereafter. This abnormal behavior can be understood using the χ_t decomposition [75]⁵.

$$\chi_t(T, \theta, \mu_5) = -\frac{1}{4}m_0\langle\bar{\psi}\psi\rangle + \frac{1}{4}m_0^2\chi_\eta(T, \theta, \mu_5), \quad (47)$$

where

$$\chi_\eta(T, \theta, \mu_5) = \int_T dx^4 \langle (\bar{\psi}i\gamma_5\psi)(\bar{\psi}(x)i\gamma_5\psi(x)) \rangle_{\theta, \mu_5}. \quad (48)$$

⁵ There is a typo in Eq. (4) of Ref. [75], where the imaginary unit i should be replaced with a minus sign.

For large enough θ , the second term in (47) becomes dominant over the first one and a χ_t peak develops due to the rapid decrease of the pseudoscalar condensate with T since $\chi_\eta \sim \frac{\partial}{\partial T}\langle\bar{\psi}i\gamma_5\psi\rangle$. This phenomenon becomes more pronounced for $\theta = \pi$ where a second order phase transition for CP restoration happens at $T = T_c$ where $|\chi_t|$ becomes divergent, as demonstrated in Panel (f). This implies that $|\chi_t|$ can become quite large for $T \sim T_c$ at $\theta = \pi$ or $\theta \sim \pi$ at $T = T_c$.

Figures 3-6 show the obtained GW signal strength versus the axionic DM annihilation temperature T_* , with the data calculated within NNJL I. The two purple lines in these figures correspond to the 2σ contour from Ref.[2], with the region inside denoting the allowed parameter space. The wiggles in the signal strength curves arise from the thresholds encoded in $g_*(T)$. Note that in all the cases, the θ range near $\theta = 0.5\pi$ can not access the two-line region since the coefficient $C(\theta)$ is quite small. Fig. 3 demonstrates that for $\mu_5 = 0$, the θ ranges $0 \leq \theta \leq 0.34\pi$ and $0.98\pi \leq \theta \leq \pi$ can en-

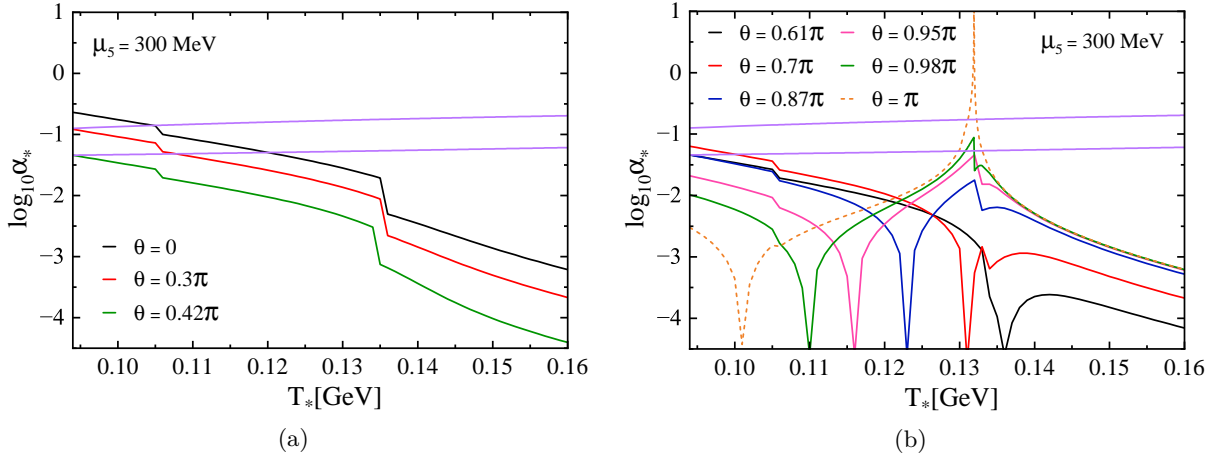


FIG. 8: Same as in Fig. 7, but for $\mu_5 = 300$ MeV. Left panel: $0 \leq \theta \leq 0.42\pi$; lower panel: $0.61\pi \leq \theta \leq 0.87\pi$ and $0.98\pi \leq \theta \leq \pi$ can access the two-line regime.

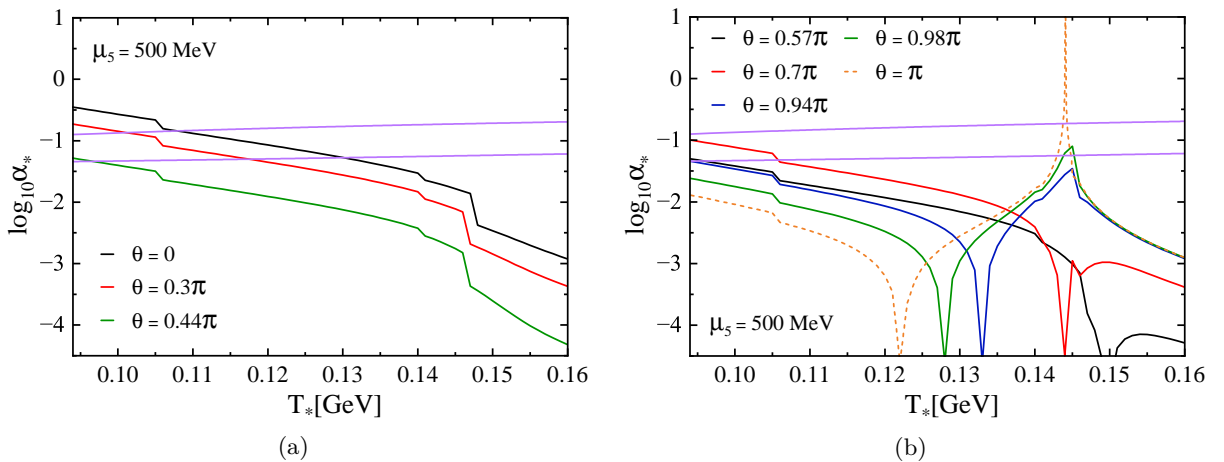


FIG. 9: Same as in Fig. 7, but for $\mu_5 = 500$ MeV. Left panel: $0 \leq \theta \leq 0.44\pi$; right panel: $0.57\pi \leq \theta \leq 0.94\pi$ and $0.98\pi \leq \theta \leq \pi$ can access the two-line regime.

ter the two-line regime: the former stems from the weaker suppression of the susceptibility at small angles and lower temperatures, while the latter results from the rapid decrease of the pseudo-scalar condensate with temperature. In the right panel of Fig. 3, each curve exhibits two peaks: the inverted one corresponds to zero χ_t and the other the maximum of $|\chi_t|$, as illustrated in panels (d)-(f) of Fig. 2. When chirality imbalance is taken into account, Figs. 4-6 show that with increasing μ_5 , the small- θ range with $\theta < 0.5\pi$ that can access the two-line regime widens, whereas the shape of the signal strength peak near $\theta = \pi$ tend to become narrower. We see that for the large chiral chemical potential $\mu_5 = 500$ MeV, in addition to $0 \leq \theta \leq 0.42\pi$ and $0.98\pi \leq \theta \leq \pi$, the interval $0.6\pi \leq \theta \leq 0.89\pi$ can also access the two-line region due to the enhanced χ_t .

The numerical results based on NNJL II-III are qualitatively consistent with those obtained within NNJL I. Here we only show the signal strength versus the axionic DW annihilation temperature

T_* calculated using NNJL II-III in Figs. 7-10 and Figs. 11-14, respectively. In the calculations, the range of μ_5 is extended to 700 MeV in NNJL II and 600 MeV in NNJL III, because the effective momentum cutoff (see Table 1) are relatively large.

Thus, in contrast to the previous study employing the local NJL formalism [75], we find that interpreting the nHz GW generation via the axionic DW collapse mechanism driven by the QCD bias remains possible, provided that the local CP-odd effect induced by the QCD sphaleron transition is taken into account. For $\mu_5 = 0$, our study suggests that beside $\theta = \pi$, the contribution to χ_t from the rapid decrease of the pseudo-scalar condensate with T becomes sizable for the range $0.5 < \theta/\pi < 1$. Note that this point is not found in Ref. [75], where only the significant enhancement of $|\chi_t|$ at the critical temperature T_c for $\theta = \pi$ is emphasized. The nonlocal NJL model study suggests that, in addition to the (T, θ) region with small θ and lower temperature, there exists a narrow (T, θ) region near (T_c, π) that can enter the

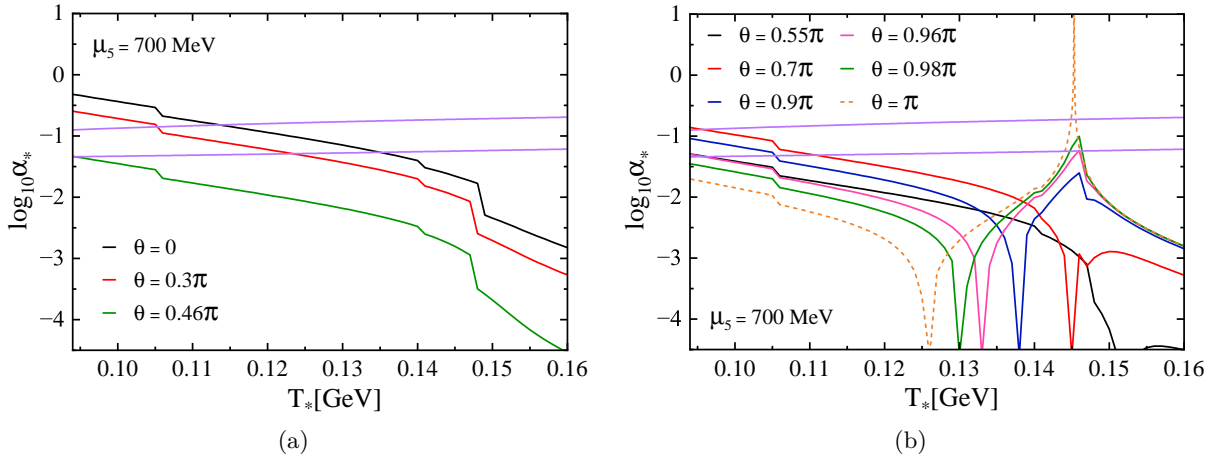


FIG. 10: Same as in Fig. 7, but for $\mu_5 = 700$ MeV. Left panel: $0 \leq \theta \leq 0.46\pi$; right panel: $0.55\pi \leq \theta \leq 0.96\pi$ and $0.98\pi \leq \theta \leq \pi$ can access the two-line regime.

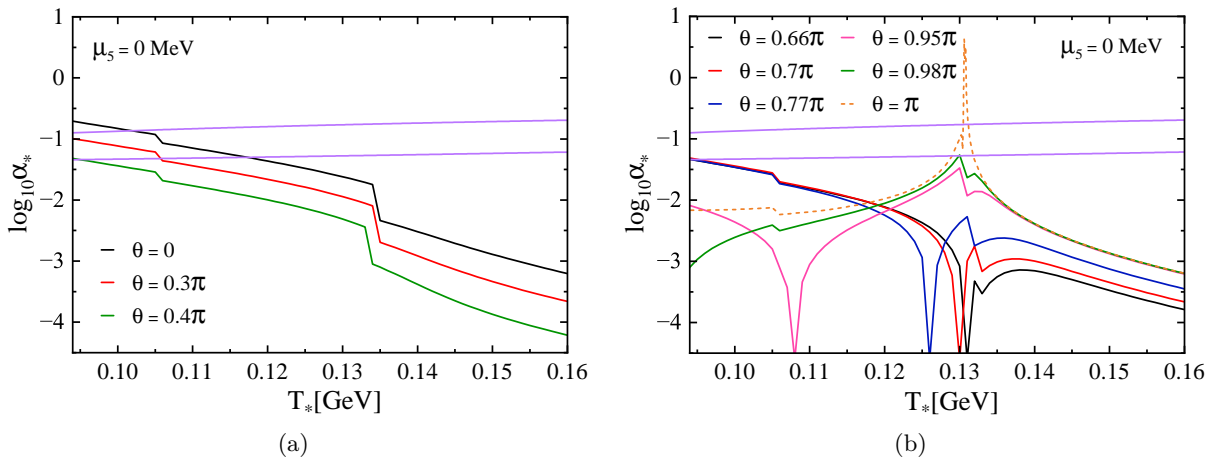


FIG. 11: Same as in Fig. 3, but within NNJL III. Left panel: $0 \leq \theta \leq 0.4\pi$; right panel: $0.67\pi \leq \theta \leq 0.77\pi$ and $0.98\pi \leq \theta \leq \pi$ can access the two-line regime.

two-line area. For nonzero μ_5 , the first region is enlarged due to the catalysis effect on the chiral condensate, while the second tends to shrink because the peak of $|\chi_t|$ becomes narrower. Further, the third region to the right of $\theta = 0.5\pi$, which supports the NG15 data, emerges as a result of the strong catalysis effect for a large enough μ_5 .

It is still difficult to estimate the possible magnitude of μ_5 in the local hot CP-odd domain during the epoch of QCD phase transition in the early Universe, just as it is in the heavy-ion collisions. The recent lattice QCD study [72] suggests that the sphaleron rate Γ_s of $N_f = 2 + 1$ QCD at $T = 230$ MeV is as large as $\Gamma_s/T^4 = 0.310$ and the extrapolated ratio at the pseudo-critical temperature $T_{pc} = 155$ MeV can reach $0.7 - 1.0$. This marks a significant step from using theoretical estimates to having genuine, non-perturbative predictions for μ_5 or the chiral charge density. From the energy scale viewpoint, if μ_5 lies within the range $0 < \mu_5 \leq \pi T_{pc} \approx 480$ MeV for T near T_{pc} , our study indicates that the θ windows for the nHz GW exist

for both the small- θ region near zero and large- θ one near $\theta = \pi$. In such cases, even if μ_5 is not necessary, it can influence the (T, θ) region for the nHz GW. On the other hand, a large $\mu_5 > \pi T_{pc}$ is necessary to balance the χ_t suppression by θ for a middle θ window with θ near but greater than 0.5π to support the NG15 data.

The effect of QCD deconfinement phase transition can be partially incorporated in the NNJL formalism by introducing the Polyakov-loop dynamics (namely the so-called PNNJL model [79]). For simplicity, we don't take into account the Polyakov-loop degrees of freedom in this work. Note that it has been demonstrated that the main conclusion obtained in the local NJL is qualitatively consistent with that from the Polyakov-loop extended NJL model (PNJL) in Ref. [75]. In particular, the sharp spike of χ_t at $\theta = \pi$ obtained in the local NJL persists in the local PNJL. We may therefore expect that our main results obtained in the NNJL model are also insensitive to the Polyakov-loop dynamics.

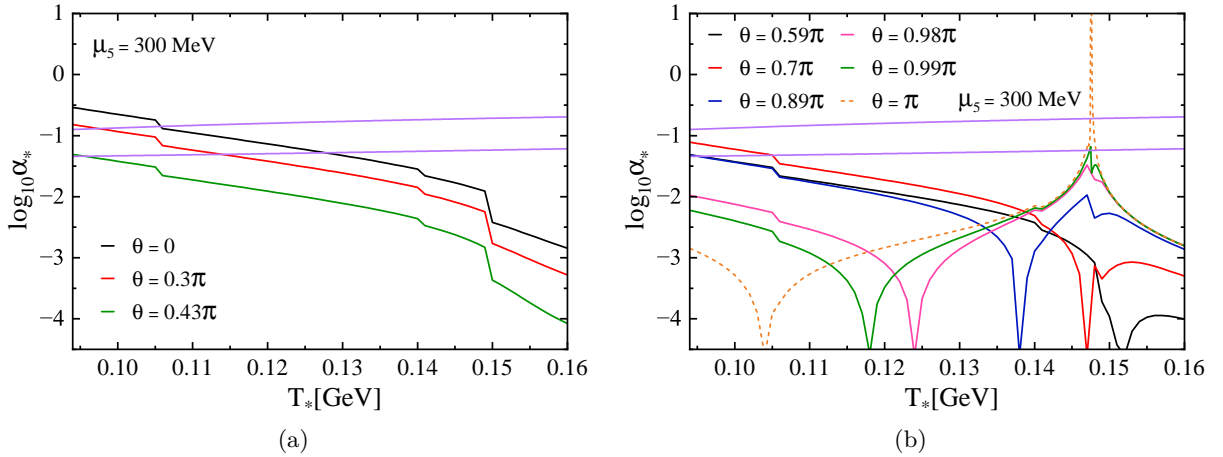


FIG. 12: Same as in Fig. 11, but for $\mu_5 = 300$ MeV. Left panel: $0 \leq \theta \leq 0.43\pi$; right panel: $0.59\pi \leq \theta \leq 0.89\pi$ and $0.99\pi \leq \theta \leq \pi$ can access the two-line regime.

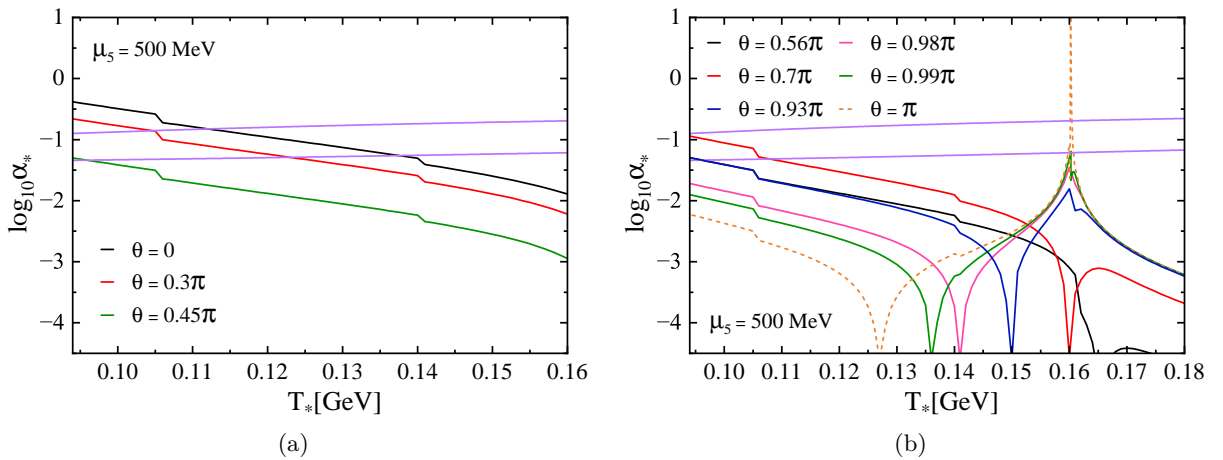


FIG. 13: Same as in Fig. 11, but for $\mu_5 = 400$ MeV. Left panel: $0 \leq \theta \leq 0.45\pi$; right panel: $0.56\pi \leq \theta \leq 0.93\pi$ and $0.99\pi \leq \theta \leq \pi$ can access the two-line regime.

V. CONCLUSIONS

In this work, we study the influence of the chirality imbalance in hot local CP-odd domain due to QCD sphaleron transitions on the possible interpretation of nHz GWs from the QCD-biased axionic DW annihilation. The bias can be attributed to the QCD topological susceptibility χ_t and its dependence on the chiral chemical potential μ_5 and the θ angle near the chiral transition temperature is calculated within the nonlocal NJL model with the instanton induced interactions. The resulting GW signal strength is then evaluated and compared to the NG15 data.

We find that even if the topological susceptibility is suppressed significantly by nonzero θ beyond the critical region for the CP restoration, the interpretation of nHz GWs generated by the QCD-biased axionic DW collapse is still possible for a certain range of θ if μ_5 is large enough, due to the catalytic effect of the chirality imbalance on χ_t . Considering the coefficient $2 \cos \theta$, the QCD bias may yield an

NG15-consistent GW signal strength for θ in the bilateral regions far from 0.5π provided that the chiral imbalance is sufficiently strong.

We confirm that for $\theta = \pi$, the topological susceptibility spike at the critical temperature T_c for the thermal CP symmetry restoration phase transition is significantly broader in the nonlocal NJL model than in the local one. Thus, for $\theta = \pi$, even if the QCD bias at $T = T_c$ produces an overly large signal strength inconsistent with the NG15 data, the χ_t -induced signal strengths near T_c can account for the generation of nHz GWs. In addition, our calculation shows that for θ near π , the χ_t as a function of T also exhibits a peak around T_c , and the resulting GW signal strengths are also consistent with the NG15 data. This point is not observed in the local NJL study [75]. Thus there exists a (θ, T) region near $\theta = \pi$ and $T = T_c$, which supports the interpretation of nHz GWs from the axionic DM annihilation. We find that such a region is suppressed by the chirality imbalance, since the aforementioned peak or spike tends to get nar-

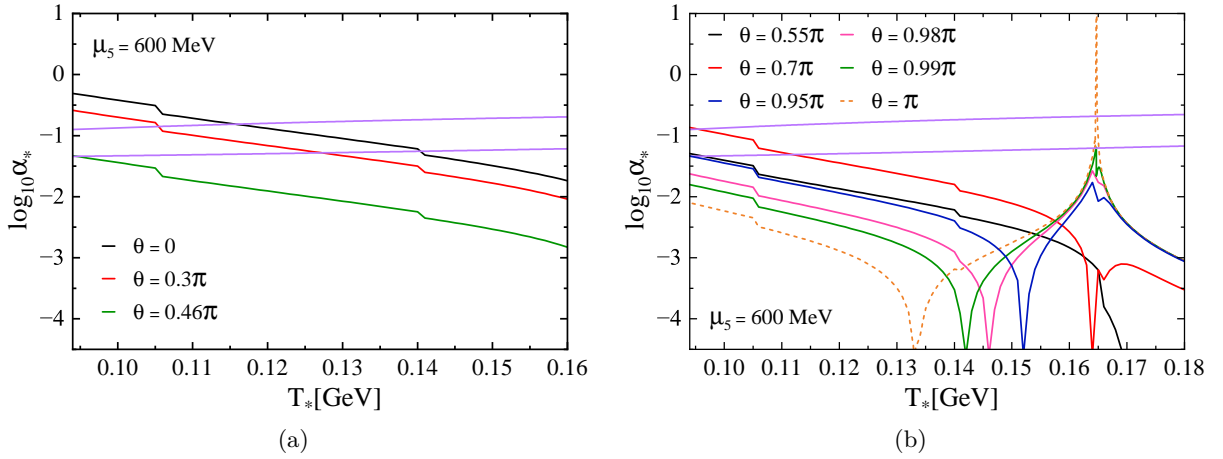


FIG. 14: Same as in Fig. 11, but for $\mu_5 = 600$ MeV. Left panel: $0 \leq \theta \leq 0.46\pi$; right panel: $0.55\pi \leq \theta \leq 0.95\pi$ and $0.99\pi \leq \theta \leq \pi$ can access the two-line regime.

rower with the increase of μ_5 .

Thus we conclude that impacts of the local CP breaking and chirality imbalance in hot QCD on the axionic DM interpretation of NG15 data are complicated. This work is limited to the mean field approximation (MFA) and two-flavor case. It is worthwhile to investigate the influence beyond the MFA and the role of the strange quark on the QCD-biased signal strength, which may alter the spike or peak structure at and around $\theta = \pi$ and $T = T_c$ altogether. Moreover, it is reported in Refs. [95, 96] that chiral imbalance can be dynamically induced by a repulsive axial-vector

interaction based on the instanton–anti-instanton molecule picture. It is also interesting to investigate how such a repulsive interaction influences the QCD-biased signal strength within the NNJL formalism.

Acknowledgements

This work was supported by the National Natural Science Foundation of China (NSFC) under Grant No. 11875127.

-
- [1] G. Agazie *et al.* [NANOGrav], “The NANOGrav 15 yr Data Set: Evidence for a Gravitational-wave Background,” *Astrophys. J. Lett.* **951**, no.1, L8 (2023) doi:10.3847/2041-8213/acdac6 [arXiv:2306.16213 [astro-ph.HE]].
- [2] A. Afzal *et al.* [NANOGrav], “The NANOGrav 15 yr Data Set: Search for Signals from New Physics,” *Astrophys. J. Lett.* **951**, no.1, L11 (2023) [erratum: *Astrophys. J. Lett.* **971**, no.1, L27 (2024); erratum: *Astrophys. J.* **971**, no.1, L27 (2024)] doi:10.3847/2041-8213/acdc91 [arXiv:2306.16219 [astro-ph.HE]].
- [3] G. Agazie *et al.* [NANOGrav], “The NANOGrav 15 yr Data Set: Constraints on Supermassive Black Hole Binaries from the Gravitational-wave Background,” *Astrophys. J. Lett.* **952**, no.2, L37 (2023) doi:10.3847/2041-8213/ace18b [arXiv:2306.16220 [astro-ph.HE]].
- [4] J. Antoniadis *et al.* [EPTA], “The second data release from the European Pulsar Timing Array - I. The dataset and timing analysis,” *Astron. Astrophys.* **678**, A48 (2023) doi:10.1051/0004-6361/202346841 [arXiv:2306.16224 [astro-ph.HE]].
- [5] J. Antoniadis *et al.* [EPTA and InPTA], *Astron. Astrophys.* **678**, A49 (2023) doi:10.1051/0004-6361/202346842 [arXiv:2306.16225 [astro-ph.HE]].
- [6] J. Antoniadis *et al.* [EPTA and InPTA:], *Astron. Astrophys.* **678**, A50 (2023) doi:10.1051/0004-6361/202346844 [arXiv:2306.16214 [astro-ph.HE]].
- [7] D. J. Reardon, A. Zic, R. M. Shannon, G. B. Hobbs, M. Bailes, V. Di Marco, A. Kapur, A. F. Rogers, E. Thrane and J. Askew, *et al.* *Astrophys. J. Lett.* **951**, no.1, L6 (2023) doi:10.3847/2041-8213/acdd02 [arXiv:2306.16215 [astro-ph.HE]].
- [8] D. J. Reardon, A. Zic, R. M. Shannon, V. Di Marco, G. B. Hobbs, A. Kapur, M. E. Lower, R. Mandow, H. Middleton and M. T. Miles, *et al.* *Astrophys. J. Lett.* **951**, no.1, L7 (2023) doi:10.3847/2041-8213/acdd03 [arXiv:2306.16229 [astro-ph.HE]].
- [9] H. Xu, S. Chen, Y. Guo, J. Jiang, B. Wang, J. Xu, Z. Xue, R. N. Caballero, J. Yuan and Y. Xu, *et al.* *Res. Astron. Astrophys.* **23**, no.7, 075024 (2023) doi:10.1088/1674-4527/acdfa5 [arXiv:2306.16216 [astro-ph.HE]].
- [10] P. Athron, C. Balázs, A. Fowlie, L. Morris and L. Wu, *Prog. Part. Nucl. Phys.* **135**, 104094 (2024) doi:10.1016/j.pnnp.2023.104094

- [arXiv:2305.02357 [hep-ph]].
- [11] J. Ellis, M. Fairbairn, G. Hütsi, J. Raidal, J. Urrutia, V. Vaskonen and H. Veermäe, *Phys. Rev. D* **109**, no.2, L021302 (2024) doi:10.1103/PhysRevD.109.L021302 [arXiv:2306.17021 [astro-ph.CO]].
- [12] Z. Q. Shen, G. W. Yuan, Y. Y. Wang and Y. Z. Wang, [arXiv:2306.17143 [astro-ph.HE]].
- [13] A. Ashoorioon, K. Rezazadeh and A. Rostami, *Phys. Lett. B* **835**, 137542 (2022) doi:10.1016/j.physletb.2022.137542 [arXiv:2202.01131 [astro-ph.CO]].
- [14] Q. Tan, Y. Wu and L. Liu, [arXiv:2411.16505 [astro-ph.CO]].
- [15] C. Han, K. P. Xie, J. M. Yang and M. Zhang, *Phys. Rev. D* **109**, no.11, 115025 (2024) doi:10.1103/PhysRevD.109.115025 [arXiv:2306.16966 [hep-ph]].
- [16] E. Megias, G. Nardini and M. Quiros, *Phys. Rev. D* **108**, no.9, 095017 (2023) doi:10.1103/PhysRevD.108.095017 [arXiv:2306.17071 [hep-ph]].
- [17] K. Fujikura, S. Girmohanta, Y. Nakai and M. Suzuki, *Phys. Lett. B* **846**, 138203 (2023) doi:10.1016/j.physletb.2023.138203 [arXiv:2306.17086 [hep-ph]].
- [18] J. Ellis and M. Lewicki, *Phys. Rev. Lett.* **126**, no.4, 041304 (2021) doi:10.1103/PhysRevLett.126.041304 [arXiv:2009.06555 [astro-ph.CO]].
- [19] Z. Y. Qiu and Z. H. Yu, *Chin. Phys. C* **47**, no.8, 085104 (2023) doi:10.1088/1674-1137/acd9bf [arXiv:2304.02506 [hep-ph]].
- [20] J. Ellis, M. Lewicki, C. Lin and V. Vaskonen, *Phys. Rev. D* **108**, no.10, 103511 (2023) doi:10.1103/PhysRevD.108.103511 [arXiv:2306.17147 [astro-ph.CO]].
- [21] Z. Wang, L. Lei, H. Jiao, L. Feng and Y. Z. Fan, *Sci. China Phys. Mech. Astron.* **66**, no.12, 120403 (2023) doi:10.1007/s11433-023-2262-0 [arXiv:2306.17150 [astro-ph.HE]].
- [22] N. Kitajima and K. Nakayama, *Phys. Lett. B* **846**, 138213 (2023) doi:10.1016/j.physletb.2023.138213 [arXiv:2306.17390 [hep-ph]].
- [23] C. W. Chiang and B. Q. Lu, *JCAP* **05**, 049 (2021) doi:10.1088/1475-7516/2021/05/049 [arXiv:2012.14071 [hep-ph]].
- [24] A. S. Sakharov, Y. N. Eroshenko and S. G. Rubin, *Phys. Rev. D* **104**, no.4, 043005 (2021) doi:10.1103/PhysRevD.104.043005 [arXiv:2104.08750 [hep-ph]].
- [25] S. F. King, D. Marfatia and M. H. Rahat, *Phys. Rev. D* **109**, no.3, 035014 (2024) doi:10.1103/PhysRevD.109.035014 [arXiv:2306.05389 [hep-ph]].
- [26] N. Kitajima, J. Lee, K. Murai, F. Takahashi and W. Yin, *Phys. Lett. B* **851**, 138586 (2024) doi:10.1016/j.physletb.2024.138586 [arXiv:2306.17146 [hep-ph]].
- [27] S. Vagnozzi, *JHEAp* **39**, 81-98 (2023) doi:10.1016/j.jheap.2023.07.001 [arXiv:2306.16912 [astro-ph.CO]].
- [28] D. Borah, S. Jyoti Das and R. Samanta, *JCAP* **03**, 031 (2024) doi:10.1088/1475-7516/2024/03/031 [arXiv:2307.00537 [hep-ph]].
- [29] K. Murai and W. Yin, *JHEP* **10**, 062 (2023) doi:10.1007/JHEP10(2023)062 [arXiv:2307.00628 [hep-ph]].
- [30] S. Datta and R. Samanta, *Phys. Rev. D* **108**, no.9, L091706 (2023) doi:10.1103/PhysRevD.108.L091706 [arXiv:2307.00646 [hep-ph]].
- [31] D. Chowdhury, G. Tasinato and I. Zavala, *JCAP* **11**, 090 (2023) doi:10.1088/1475-7516/2023/11/090 [arXiv:2307.01188 [hep-th]].
- [32] Z. Yi, Z. Q. You and Y. Wu, *JCAP* **01**, 066 (2024) doi:10.1088/1475-7516/2024/01/066 [arXiv:2308.05632 [astro-ph.CO]].
- [33] S. Wang, Z. C. Zhao, J. P. Li and Q. H. Zhu, *Phys. Rev. Res.* **6**, no.1, L012060 (2024) doi:10.1103/PhysRevResearch.6.L012060 [arXiv:2307.00572 [astro-ph.CO]].
- [34] L. Liu, Z. C. Chen and Q. G. Huang, *Phys. Rev. D* **109**, no.6, 6 (2024) doi:10.1103/PhysRevD.109.L061301 [arXiv:2307.01102 [astro-ph.CO]].
- [35] D. G. Figueroa, M. Pieroni, A. Ricciardone and P. Simakachorn, *Phys. Rev. Lett.* **132**, no.17, 171002 (2024) doi:10.1103/PhysRevLett.132.171002 [arXiv:2307.02399 [astro-ph.CO]].
- [36] Z. Yi, Q. Gao, Y. Gong, Y. Wang and F. Zhang, *Sci. China Phys. Mech. Astron.* **66**, no.12, 120404 (2023) doi:10.1007/s11433-023-2266-1 [arXiv:2307.02467 [gr-qc]].
- [37] G. Lambiase, L. Mastrototaro and L. Visinelli, *Phys. Rev. D* **108**, no.12, 123028 (2023) doi:10.1103/PhysRevD.108.123028 [arXiv:2306.16977 [astro-ph.HE]].
- [38] J. Yang, N. Xie and F. P. Huang, *JCAP* **11**, 045 (2024) doi:10.1088/1475-7516/2024/11/045 [arXiv:2306.17113 [hep-ph]].
- [39] H. Deng, B. Bécsy, X. Siemens, N. J. Cornish and D. R. Madison, *Phys. Rev. D* **108**, no.10, 102007 (2023) doi:10.1103/PhysRevD.108.102007 [arXiv:2306.17130 [gr-qc]].
- [40] G. Franciolini, D. Racco and F. Rompineve, *Phys. Rev. Lett.* **132**, no.8, 081001 (2024) [erratum: *Phys. Rev. Lett.* **133**, no.18, 189901 (2024)] doi:10.1103/PhysRevLett.132.081001 [arXiv:2306.17136 [astro-ph.CO]].
- [41] G. Franciolini, A. Iovino, Junior., V. Vaskonen and H. Veermäe, *Phys. Rev. Lett.* **131**, no.20, 201401 (2023) doi:10.1103/PhysRevLett.131.201401 [arXiv:2306.17149 [astro-ph.CO]].
- [42] T. W. B. Kibble, *J. Phys. A* **9**, 1387-1398 (1976) doi:10.1088/0305-4470/9/8/029
- [43] Y. B. Zeldovich, I. Y. Kobzarev and L. B. Okun, *Zh. Eksp. Teor. Fiz.* **67**, 3-11 (1974) SLAC-TRANS-0165.
- [44] B. Barman, D. Borah, S. Jyoti Das and I. Saha, *JCAP* **10**, 053 (2023) doi:10.1088/1475-7516/2023/10/053 [arXiv:2307.00656 [hep-ph]].
- [45] R. D. Peccei and H. R. Quinn, *Phys. Rev. Lett.* **38**, 1440-1443 (1977) doi:10.1103/PhysRevLett.38.1440
- [46] R. D. Peccei and H. R. Quinn, *Phys. Rev. D* **16**, 1791-1797 (1977) doi:10.1103/PhysRevD.16.1791
- [47] F. Wilczek, *Phys. Rev. Lett.* **40**, 279-282 (1978) doi:10.1103/PhysRevLett.40.279
- [48] A. Arvanitaki, S. Dimopoulos,

- S. Dubovsky, N. Kaloper and J. March-Russell, *Phys. Rev. D* **81**, 123530 (2010) doi:10.1103/PhysRevD.81.123530 [arXiv:0905.4720 [hep-th]].
- [49] B. Holdom and M. E. Peskin, *Nucl. Phys. B* **208**, 397-412 (1982) doi:10.1016/0550-3213(82)90228-0
- [50] K. Choi and H. D. Kim, *Phys. Rev. D* **59**, 072001 (1999) doi:10.1103/PhysRevD.59.072001 [arXiv:hep-ph/9809286 [hep-ph]].
- [51] Z. Zhang, C. Cai, Y. H. Su, S. Wang, Z. H. Yu and H. H. Zhang, *Phys. Rev. D* **108**, no.9, 095037 (2023) doi:10.1103/PhysRevD.108.095037 [arXiv:2307.11495 [hep-ph]].
- [52] S. Blasi, A. Mariotti, A. Rase and A. Sevrin, *JHEP* **11**, 169 (2023) doi:10.1007/JHEP11(2023)169 [arXiv:2306.17830 [hep-ph]].
- [53] H. J. Li and Y. F. Zhou, *Chin. Phys. C* **49**, no.3, 035101 (2025) doi:10.1088/1674-1137/ada003 [arXiv:2401.09138 [hep-ph]].
- [54] J. Ellis, M. Fairbairn, G. Franciolini, G. Hütsi, A. Iovino, M. Lewicki, M. Raidal, J. Urrutia, V. Vaskonen and H. Veermäe, *Phys. Rev. D* **109**, no.2, 023522 (2024) doi:10.1103/PhysRevD.109.023522 [arXiv:2308.08546 [astro-ph.CO]].
- [55] K. D. Lozanov, S. Pi, M. Sasaki, V. Takhistov and A. Wang, *Class. Quant. Grav.* **42**, no.3, 035007 (2025) doi:10.1088/1361-6382/ad9e67 [arXiv:2310.03594 [astro-ph.CO]].
- [56] G. B. Gelmini and J. Hyman, *Phys. Lett. B* **848**, 138356 (2024) doi:10.1016/j.physletb.2023.138356 [arXiv:2307.07665 [hep-ph]].
- [57] M. Geller, S. Ghosh, S. Lu and Y. Tsai, *Phys. Rev. D* **109**, no.6, 063537 (2024) doi:10.1103/PhysRevD.109.063537 [arXiv:2307.03724 [hep-ph]].
- [58] Y. Bai, T. K. Chen and M. Korwar, *JHEP* **12**, 194 (2023) doi:10.1007/JHEP12(2023)194 [arXiv:2306.17160 [hep-ph]].
- [59] S. Borsanyi, Z. Fodor, J. Guenther, K. H. Kampert, S. D. Katz, T. Kawanai, T. G. Kovacs, S. W. Mages, A. Pasztor and F. Pittler, *et al. Nature* **539**, no.7627, 69-71 (2016) doi:10.1038/nature20115 [arXiv:1606.07494 [hep-lat]].
- [60] N. S. Manton, *Phys. Rev. D* **28**, 2019 (1983) doi:10.1103/PhysRevD.28.2019
- [61] F. R. Klinkhamer and N. S. Manton, *Phys. Rev. D* **30**, 2212 (1984) doi:10.1103/PhysRevD.30.2212
- [62] V. A. Kuzmin, V. A. Rubakov and M. E. Shaposhnikov, *Phys. Lett. B* **155**, 36 (1985) doi:10.1016/0370-2693(85)91028-7
- [63] M. E. Shaposhnikov, *Nucl. Phys. B* **287**, 757-775 (1987) doi:10.1016/0550-3213(87)90127-1
- [64] S. Y. Khlebnikov and M. E. Shaposhnikov, *Nucl. Phys. B* **308**, 885-912 (1988) doi:10.1016/0550-3213(88)90133-2
- [65] P. B. Arnold and L. D. McLerran, *Phys. Rev. D* **36**, 581 (1987) doi:10.1103/PhysRevD.36.581
- [66] P. B. Arnold and L. D. McLerran, *Phys. Rev. D* **37**, 1020 (1988) doi:10.1103/PhysRevD.37.1020
- [67] L. D. McLerran, E. Mottola and M. E. Shaposhnikov, *Phys. Rev. D* **43**, 2027-2035 (1991) doi:10.1103/PhysRevD.43.2027
- [68] G. D. Moore, *Phys. Lett. B* **412**, 359-370 (1997) doi:10.1016/S0370-2693(97)01046-0 [arXiv:hep-ph/9705248 [hep-ph]].
- [69] G. D. Moore and K. Rummukainen, *Phys. Rev. D* **61**, 105008 (2000) doi:10.1103/PhysRevD.61.105008 [arXiv:hep-ph/9906259 [hep-ph]].
- [70] G. D. Moore and M. Tassler, *JHEP* **02**, 105 (2011) doi:10.1007/JHEP02(2011)105 [arXiv:1011.1167 [hep-ph]].
- [71] M. Barroso Mancha and G. D. Moore, *JHEP* **01**, 155 (2023) doi:10.1007/JHEP01(2023)155 [arXiv:2210.05507 [hep-lat]].
- [72] C. Bonanno, F. D'Angelo, M. D'Elia, L. Maio and M. Naviglio, *Phys. Rev. Lett.* **132**, no.5, 051903 (2024) doi:10.1103/PhysRevLett.132.051903 [arXiv:2308.01287 [hep-lat]].
- [73] D. E. Kharzeev, L. D. McLerran and H. J. Warringa, *Nucl. Phys. A* **803**, 227-253 (2008) doi:10.1016/j.nuclphysa.2008.02.298 [arXiv:0711.0950 [hep-ph]].
- [74] K. Fukushima, D. E. Kharzeev and H. J. Warringa, *Phys. Rev. D* **78**, 074033 (2008) doi:10.1103/PhysRevD.78.074033 [arXiv:0808.3382 [hep-ph]].
- [75] L. Huang, Y. Wang, H. X. Zhang, S. Matsuzaki, H. Ishida, M. Kawaguchi and A. Tomiya, *Phys. Rev. D* **109**, no.11, 115015 (2024) doi:10.1103/PhysRevD.109.115015 [arXiv:2403.11444 [hep-ph]].
- [76] N. Y. Astrakhantsev, V. V. Braguta, A. Y. Kotov, D. D. Kuznedev and A. A. Nikolaev, *Eur. Phys. J. A* **57**, no.1, 15 (2021) doi:10.1140/epja/s10050-020-00326-2 [arXiv:1902.09325 [hep-lat]].
- [77] V. V. Braguta, E. M. Ilgenfritz, A. Y. Kotov, B. Petersson and S. A. Skinderev, *Phys. Rev. D* **93**, no.3, 034509 (2016) doi:10.1103/PhysRevD.93.034509 [arXiv:1512.05873 [hep-lat]].
- [78] V. V. Braguta, V. A. Goy, E. M. Ilgenfritz, A. Y. Kotov, A. V. Molochkov, M. Muller-Preussker and B. Petersson, *JHEP* **06**, 094 (2015) doi:10.1007/JHEP06(2015)094 [arXiv:1503.06670 [hep-lat]].
- [79] T. Hell, S. Roessner, M. Cristoforetti and W. Weise, *Phys. Rev. D* **79**, 014022 (2009) doi:10.1103/PhysRevD.79.014022 [arXiv:0810.1099 [hep-ph]].
- [80] V. P. Pagura, D. Gomez Dumm, S. Noguera and N. N. Scoccola, *Phys. Rev. D* **95**, no.3, 034013 (2017) doi:10.1103/PhysRevD.95.034013 [arXiv:1609.02025 [hep-ph]].
- [81] D. Gomez Dumm, D. B. Blaschke, A. G. Grunfeld and N. N. Scoccola, *Phys. Rev. D* **73**, 114019 (2006) doi:10.1103/PhysRevD.73.114019 [arXiv:hep-ph/0512218 [hep-ph]].
- [82] T. Hell, S. Rossner, M. Cristoforetti and W. Weise, *Phys. Rev. D* **81**, 074034 (2010) doi:10.1103/PhysRevD.81.074034 [arXiv:0911.3510 [hep-ph]].
- [83] M. Ruggieri and G. X. Peng, *J. Phys. G* **43**, no.12, 125101 (2016) doi:10.1088/0954-3899/43/12/125101 [arXiv:1602.05250 [hep-ph]].
- [84] M. Ruggieri, M. N. Chernodub and Z. Y. Lu, *Phys. Rev. D* **102**, no.1, 014031 (2020) doi:10.1103/PhysRevD.102.014031 [arXiv:2004.09393 [hep-ph]].

- [85] D. Blaschke, M. Buballa, A. E. Radzhabov and M. K. Volkov, *Yad. Fiz.* **71**, 2012-2018 (2008) doi:10.1134/S1063778808110161 [arXiv:0705.0384 [hep-ph]].
- [86] M. Frasca, *Phys. Rev. C* **84**, 055208 (2011) doi:10.1103/PhysRevC.84.055208 [arXiv:1105.5274 [hep-ph]].
- [87] M. Frasca, *Eur. Phys. J. C* **78**, no.9, 790 (2018) doi:10.1140/epjc/s10052-018-6200-7 [arXiv:1602.04654 [hep-ph]].
- [88] K. Saikawa, *Universe* **3**, no.2, 40 (2017) doi:10.3390/universe3020040 [arXiv:1703.02576 [hep-ph]].
- [89] T. Hiramatsu, M. Kawasaki and K. Saikawa, *JCAP* **05**, 032 (2010) doi:10.1088/1475-7516/2010/05/032 [arXiv:1002.1555 [astro-ph.CO]].
- [90] S. Navas *et al.* [Particle Data Group], *Phys. Rev. D* **110**, no.3, 030001 (2024) doi:10.1103/PhysRevD.110.030001
- [91] Z. Y. Lu and M. Ruggieri, *Phys. Rev. D* **100**, no.1, 014013 (2019) doi:10.1103/PhysRevD.100.014013 [arXiv:1811.05102 [hep-ph]].
- [92] D. Gomez Dumm, A. G. Grunfeld and N. N. Scoccola, *Phys. Rev. D* **74**, 054026 (2006) doi:10.1103/PhysRevD.74.054026 [arXiv:hep-ph/0607023 [hep-ph]].
- [93] A. Abhishek, A. Das, H. Mishra and R. K. Mohapatra, *Phys. Rev. D* **103**, no.7, 074003 (2021) doi:10.1103/PhysRevD.103.074003 [arXiv:2006.15727 [hep-ph]].
- [94] Z. Zhang and W. Zhao, *Phys. Rev. D* **111**, no.9, 094043 (2025) doi:10.1103/PhysRevD.111.094043 [arXiv:2501.04560 [hep-ph]].
- [95] Z. Zhang, *Phys. Rev. D* **85**, 114028 (2012) doi:10.1103/PhysRevD.85.114028 [arXiv:1201.0422 [hep-ph]].
- [96] L. Yu, H. Liu and M. Huang, *Phys. Rev. D* **90**, no.7, 074009 (2014) doi:10.1103/PhysRevD.90.074009 [arXiv:1404.6969 [hep-ph]].